Supporting Information

Impact of central atom and halido ligand on structure, antiproliferative activity and selectivity of half-sandwich Ru(II) and Ir(III) complexes with a 1,3,4-thiadiazole-based ligand

Radka Křikavová,[a*] Michaela Romanovová,[b] Zuzana Jendželovská,[b] Martin Majerník,[b] Lukáš Masaryk,[a] Pavel Zoufalý,[a] David Milde,[c] Jan Moncol,[d] Radovan Herchel,[a] Rastislav Jendželovský[b] and Ivan Nemec[a,e]

[a] *Department of Inorganic Chemistry, Faculty of Science, Palacký University Olomouc, 17. listopadu 12, CZ-771 46 Olomouc, Czech Republic*

[b] *Department of Cellular Biology, Institute of Biology and Ecology, Faculty of Science, Pavol Jozef Šafárik University in Košice, Šrobárova 2, 041 54 Košice, Slovakia*

[c] *Department of Analytical Chemistry, Faculty of Science, Palacký University Olomouc, 17. listopadu 12, CZ-771 46 Olomouc, Czech Republic*

[d] *Department of Inorganic Chemistry, Faculty of Chemical and Food Technology, Slovak University of Technology in Bratislava, Bratislava SK-81237, Slovakia*

[e] *Central European Institute of Technology, Brno University of Technology, Purkyňova 123, 61200 Brno, Czech Republic*

Table of Contents

* Corresponding Author:

(RK): E-mail: radka.krikavova@upol.cz

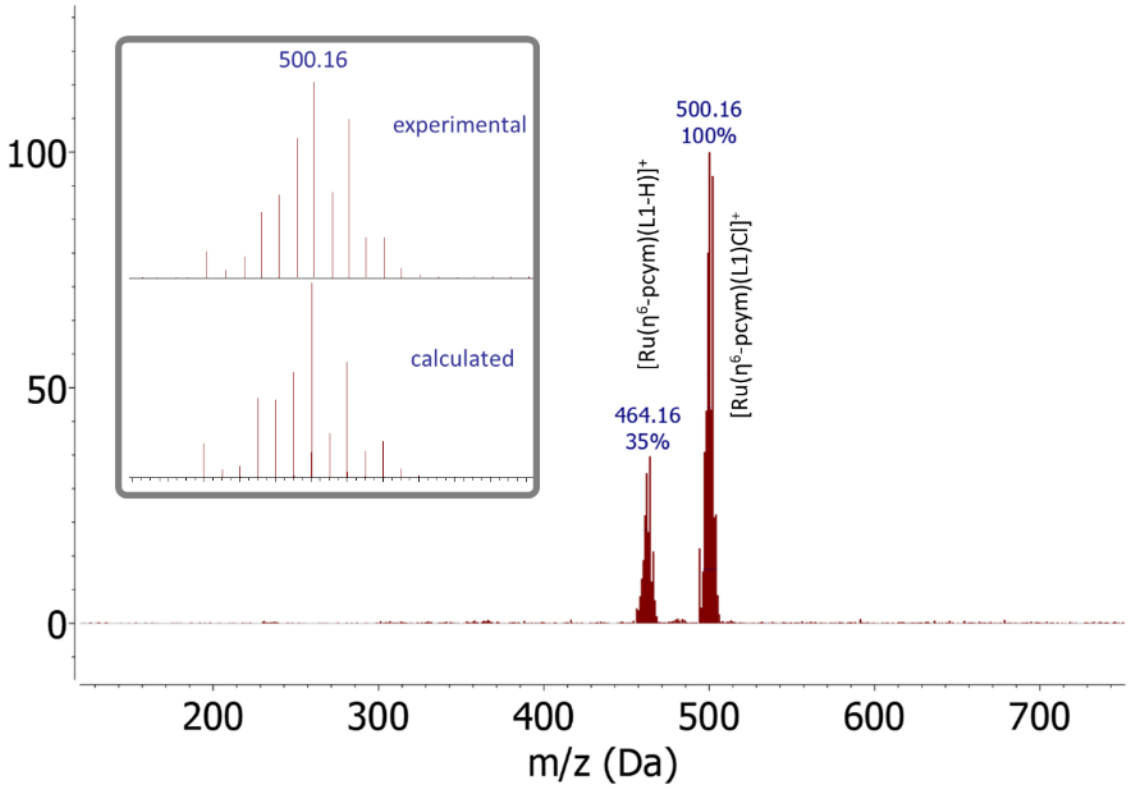

Fig. S1. ESI+ MS spectrum of complex **1** given with a comparison of the experimental and calculated isotopic distributions of the $[Ru(\eta^6\text{-pcym})(L1)Cl]^+$ species (inset).

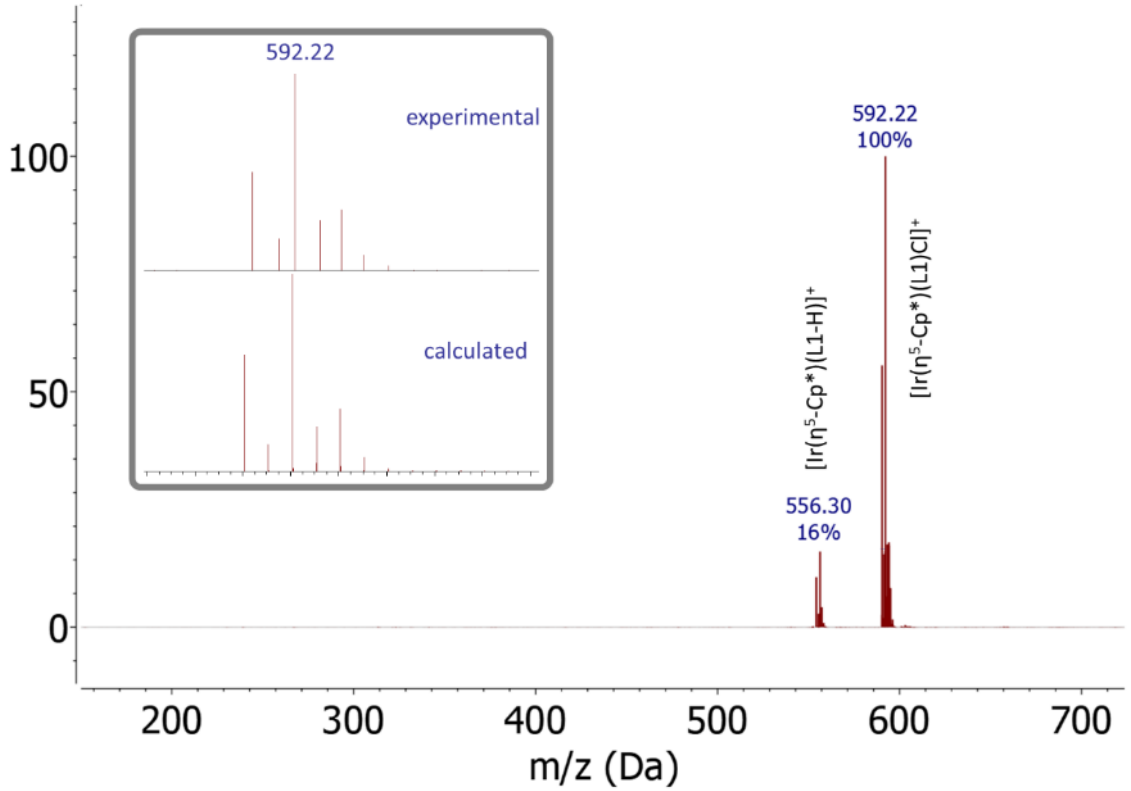

Fig. S2. ESI+ MS spectrum of complex **2** given with a comparison of the experimental and calculated isotopic distributions of the $[Ir(\eta^5\text{-Cp*})(L1)Cl]^+$ species (inset).

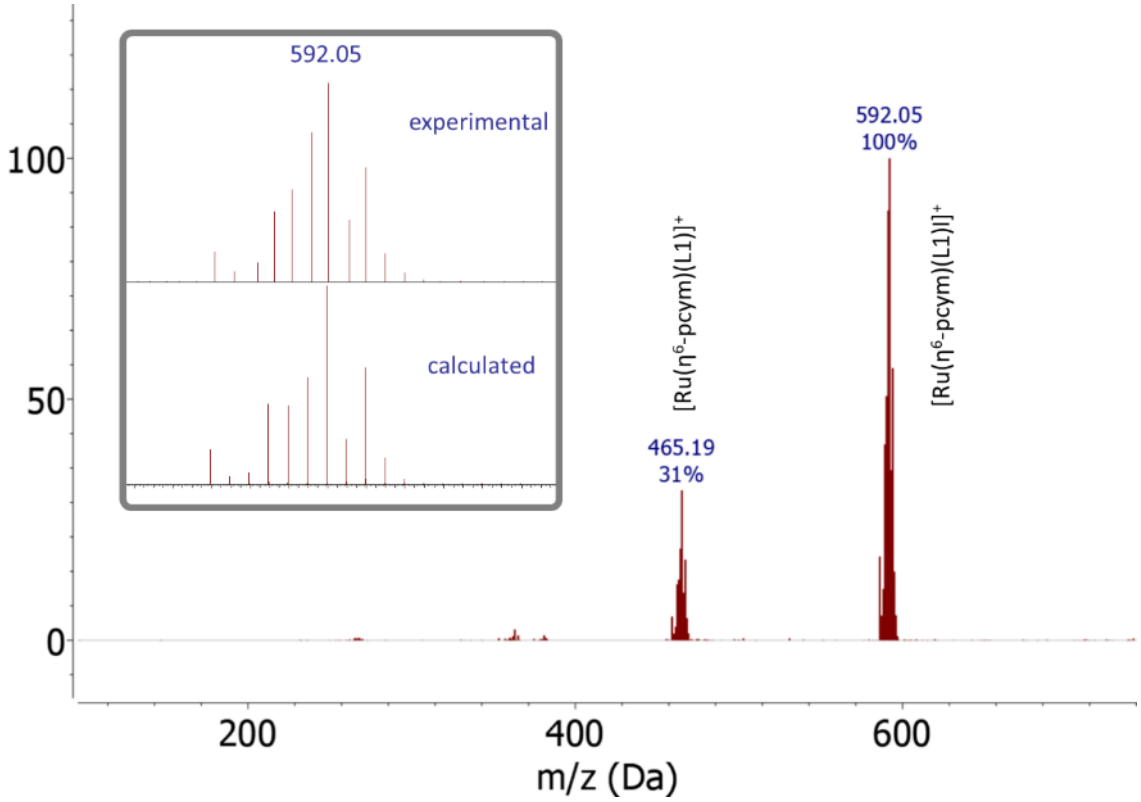

Fig. S3. ESI+ MS spectrum of complex **3** given with a comparison of the experimental and calculated isotopic distributions of the $[Ru(\eta^6\text{-pcym})(L1)I]^+$ species (inset).

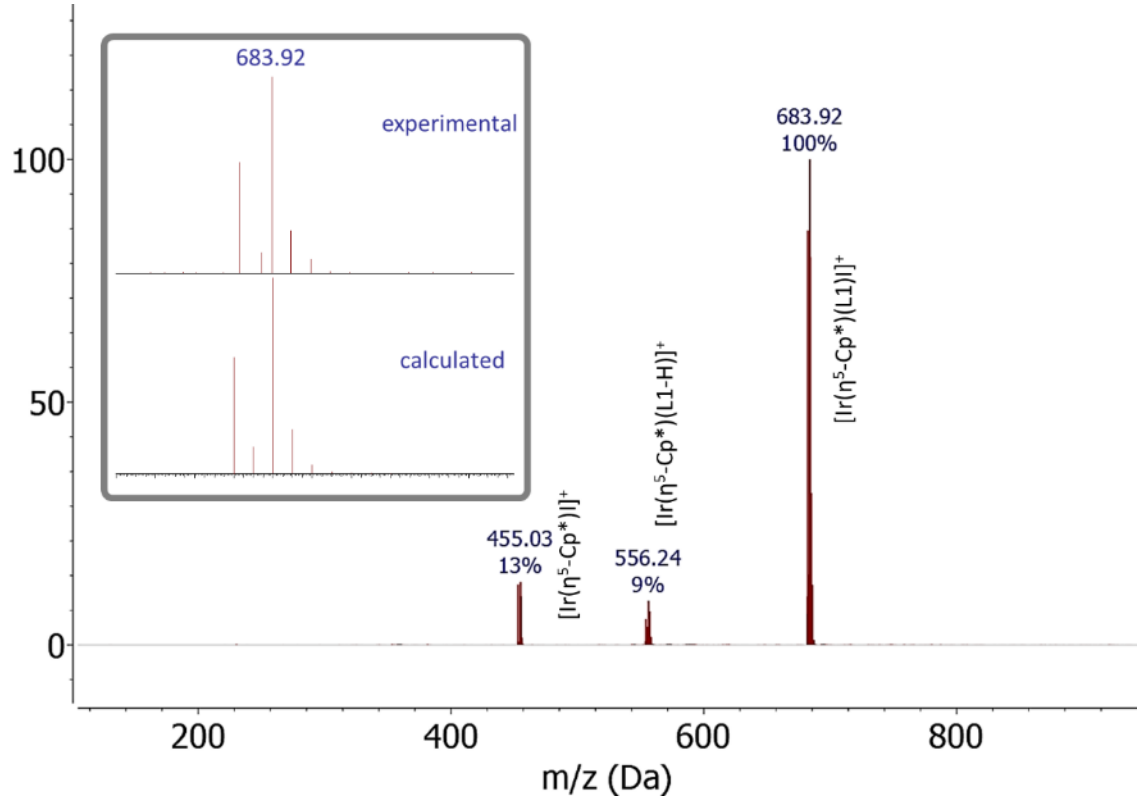

Fig. S4. ESI+ MS spectrum of complex **4** given with a comparison of the experimental and calculated isotopic distributions of the $[Ir(\eta^5\text{-Cp*})(L1)I]^+$ species (inset).

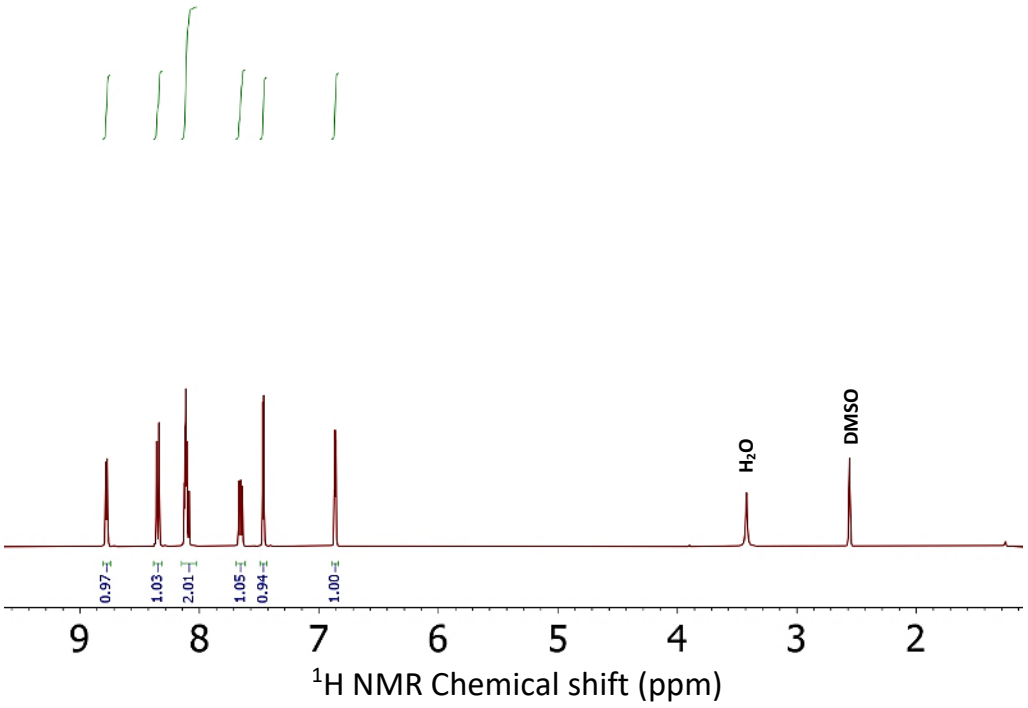

Fig. S5. ^{1}H NMR spectrum of ligand L1 in DMSO-d_6.

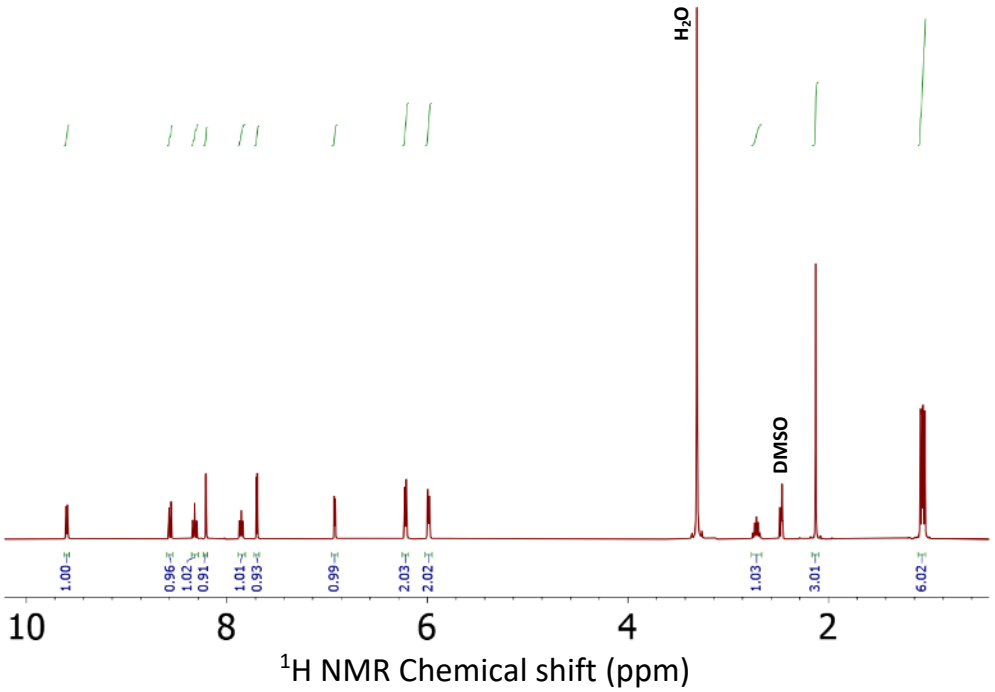

Fig. S6. ^{1}H NMR spectrum of complex **1** in DMSO-d_6.

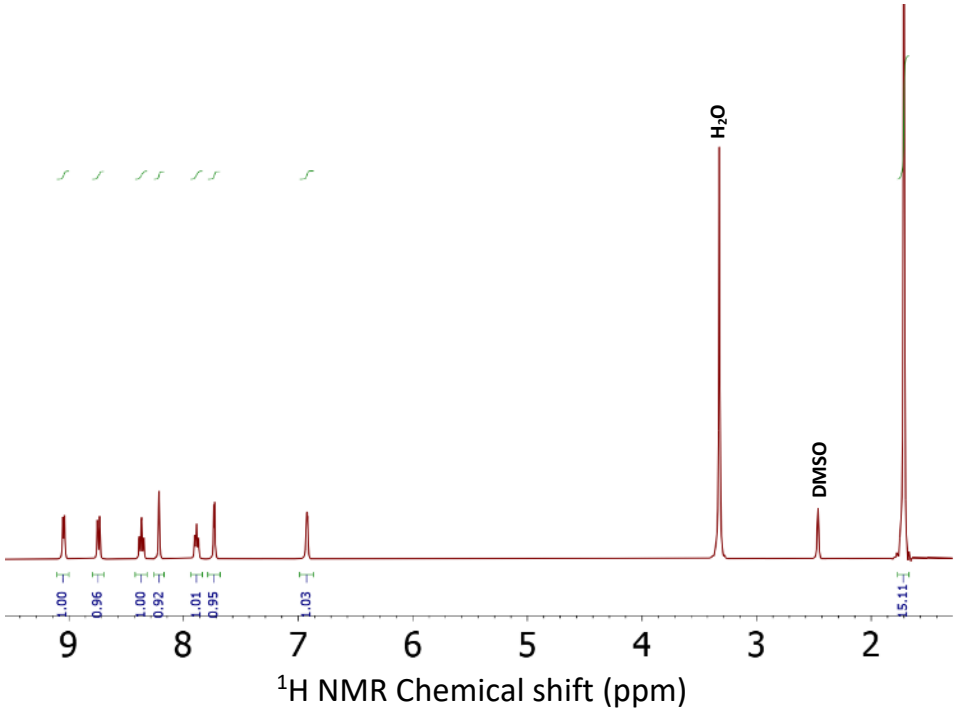

Fig. S7. ^{1}H NMR spectrum of complex **2** in DMSO-d_6.

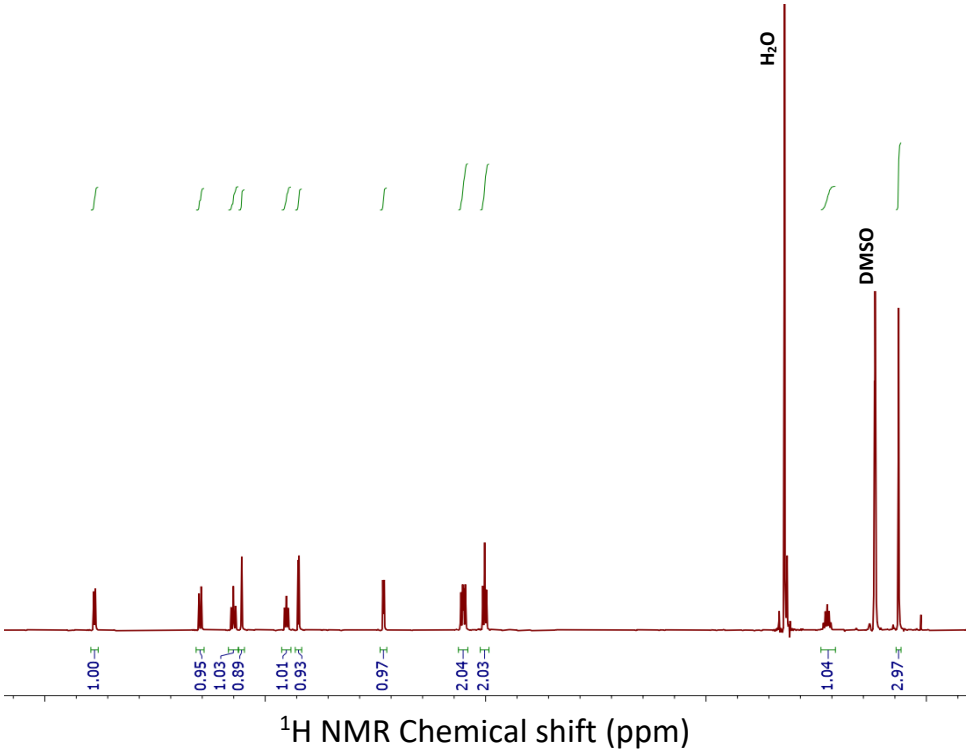

Fig. S8. ^{1}H NMR spectrum of complex **3** in DMSO-d_6.

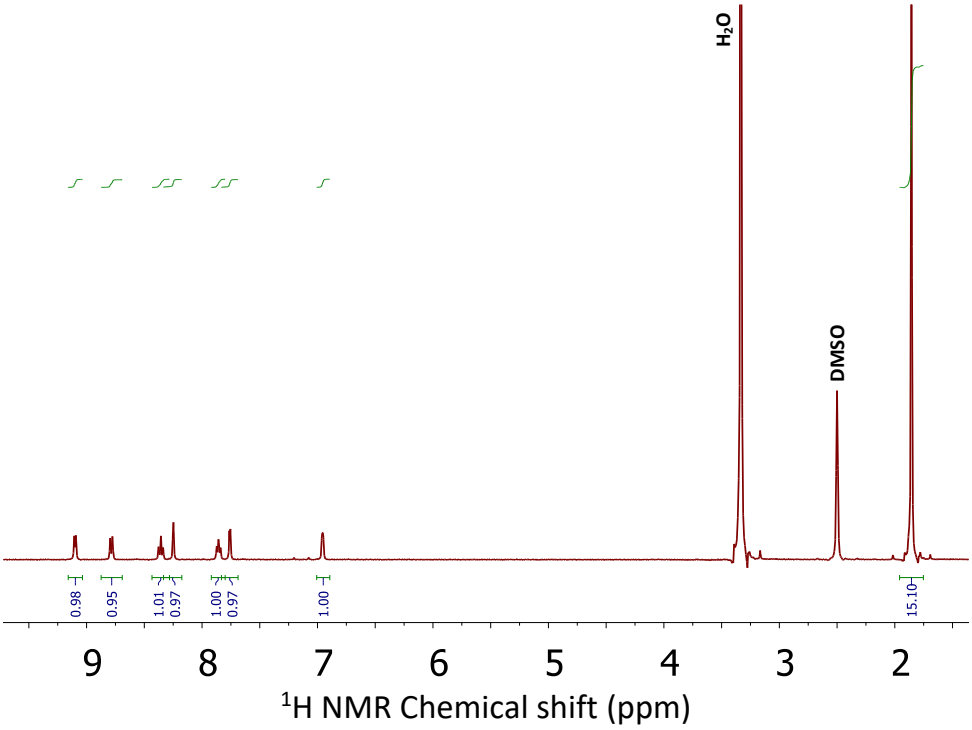

Fig. S9. ^{1}H NMR spectrum of complex **4** in DMSO-d_6.

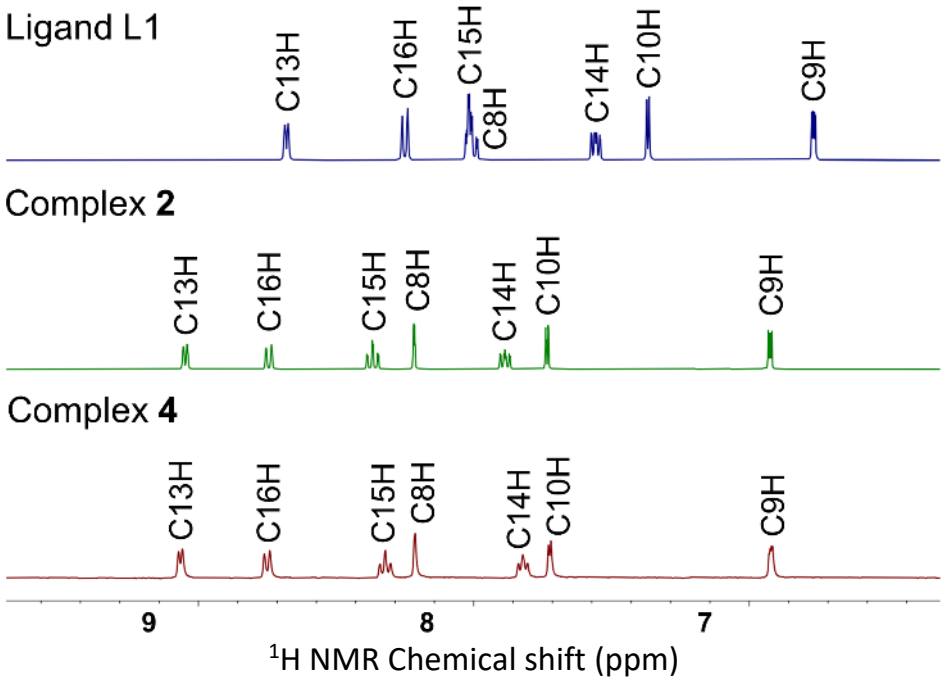

Fig. S10. Comparison of ^{1}H NMR spectra of ligand L1 (*top*) and complexes **2** and **4** (*middle* and *bottom*) in DMSO-d_6.

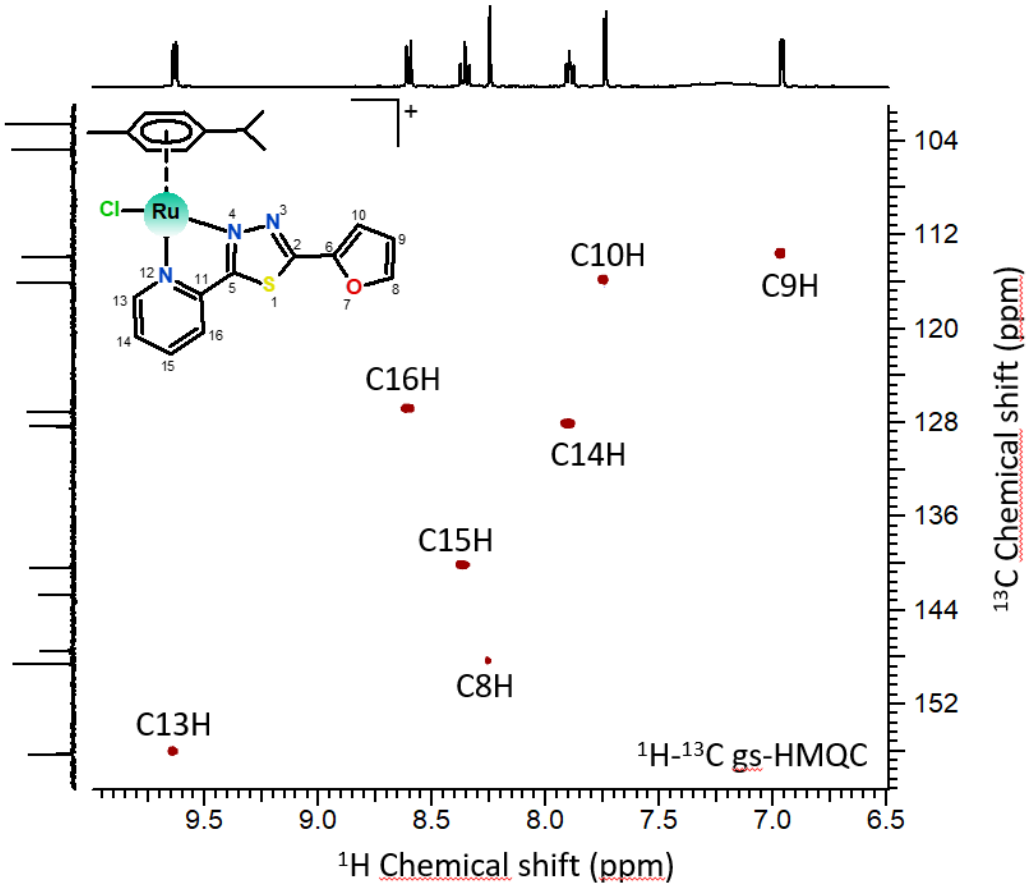

Fig. S11. A part of ^{1}H-^{13}C gs-HMQC NMR spectrum of complex **1** in DMSO-d_6 showing the signals of coordinated L1.

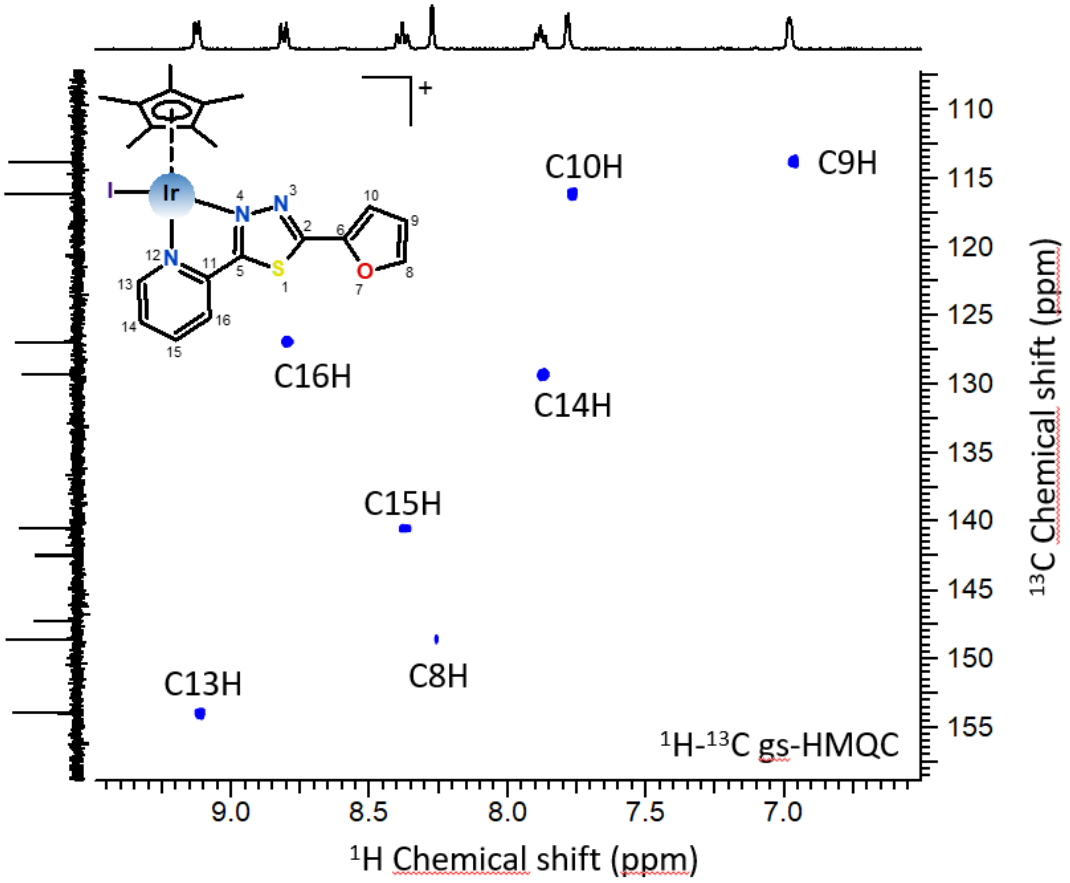

Fig. S12. A part of ^{1}H-^{13}C gs-HMQC NMR spectrum of complex **4** in DMSO-d_6 showing the signals of coordinated L1.

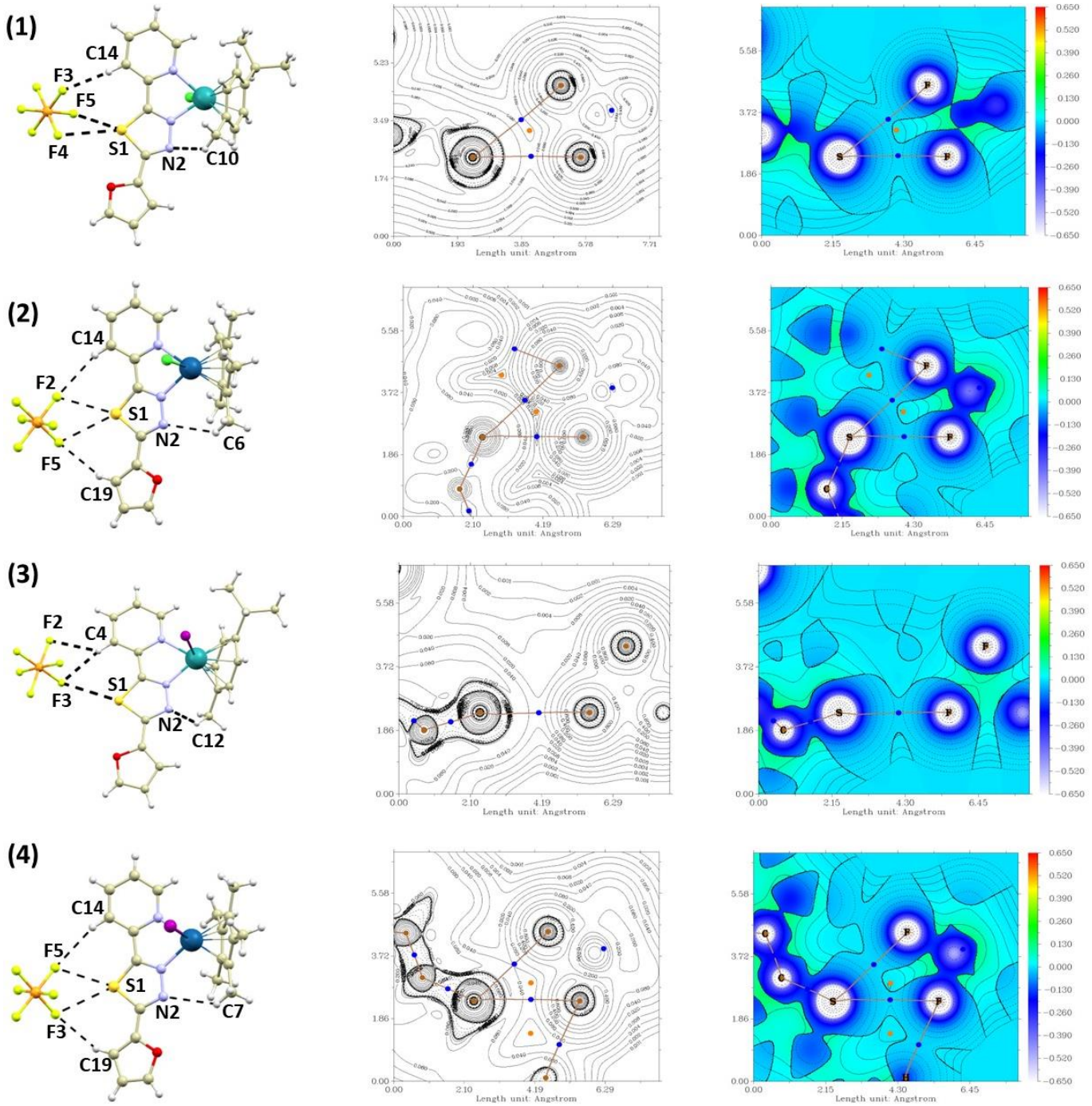

Fig. S13. A perspective view on the non-covalent interactions (black dashed lines) involving PF_6^- anions (*Left column*). The $\nabla^2\rho(\mathbf{r})$ contour (*middle column*) and signλ (*right column*) plots calculated for **1**-**4**. Blue dots represent (3,-1) critical points, orange dots represent (3,+1) ring critical points and brown dots represents (3,-3) atomic critical points. Brown lines represent bond paths. Atom labelling is provided only in the signλ plots however, view direction in the $\nabla^2\rho(\mathbf{r})$ contour plot is identical. The parameters of the depicted non-covalent interactions (in Å) and their interaction energies (E_{int} in kcal/mol): **1**, *d*(C10···N2) = 3.300(8), E_{int} = 1.49, *d*(C14···F3) = 3.451(9), E_{int} = 2.27, *d*(F4···S1) = 3.246(7), E_{int} = 1.00, *d*(F5···S1) = 3.422(6), E_{int} = 0.69; **2**, *d*(C10···N2) = 3.377(6), E_{int} = 1.58, *d*(C14···F2) = 3.688(6), E_{int} = 0.78, *d*(C19···F5) = 3.434(6), E_{int} = 1.20, *d*(F2···S1) = 3.024(3), E_{int} = 1.89, *d*(F5···S1) = 3.156(4), E_{int} = 1.31; **3**, *d*(C12···N2) = 3.300(8), E_{int} = 2.32, *d*(C4···F2) = 3.314(6), E_{int} = 1.32, *d*(C4···F3) = 3.398(5), E_{int} = 1.29, *d*(F3···S1) = 3.212(4), E_{int} = 1.08, **4**, *d*(C7···N2) = 3.422(8), E_{int} = 1.59, *d*(C14···F5) = 3.660(6), E_{int} = 0.87, *d*(C19···F3) = 3.459(8), E_{int} = 1.33, *d*(F3···S1) = 3.156(8), E_{int} = 1.31, *d*(F5···S1) = 3.025(7), E_{int} = 1.89.

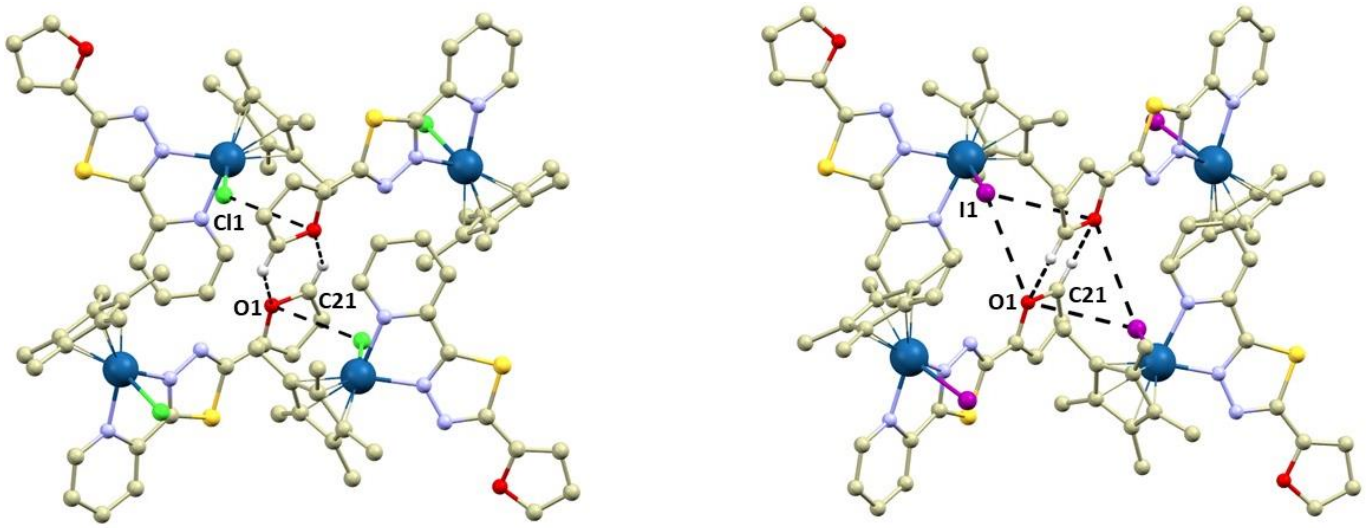

Fig. S14. A perspective view on the non-covalent interactions (black dashed lines) in **2** (*left*) and **4** (*right*). The selected donor···acceptor distances (in Å): **2**, *d*(C21···O1) = 3.406(7), *d*(Cl1···O1) = 3.670(4); **4**, *d*(C21···O1) = 3.580(18), *d*(I1···O1) = 3.668(8).

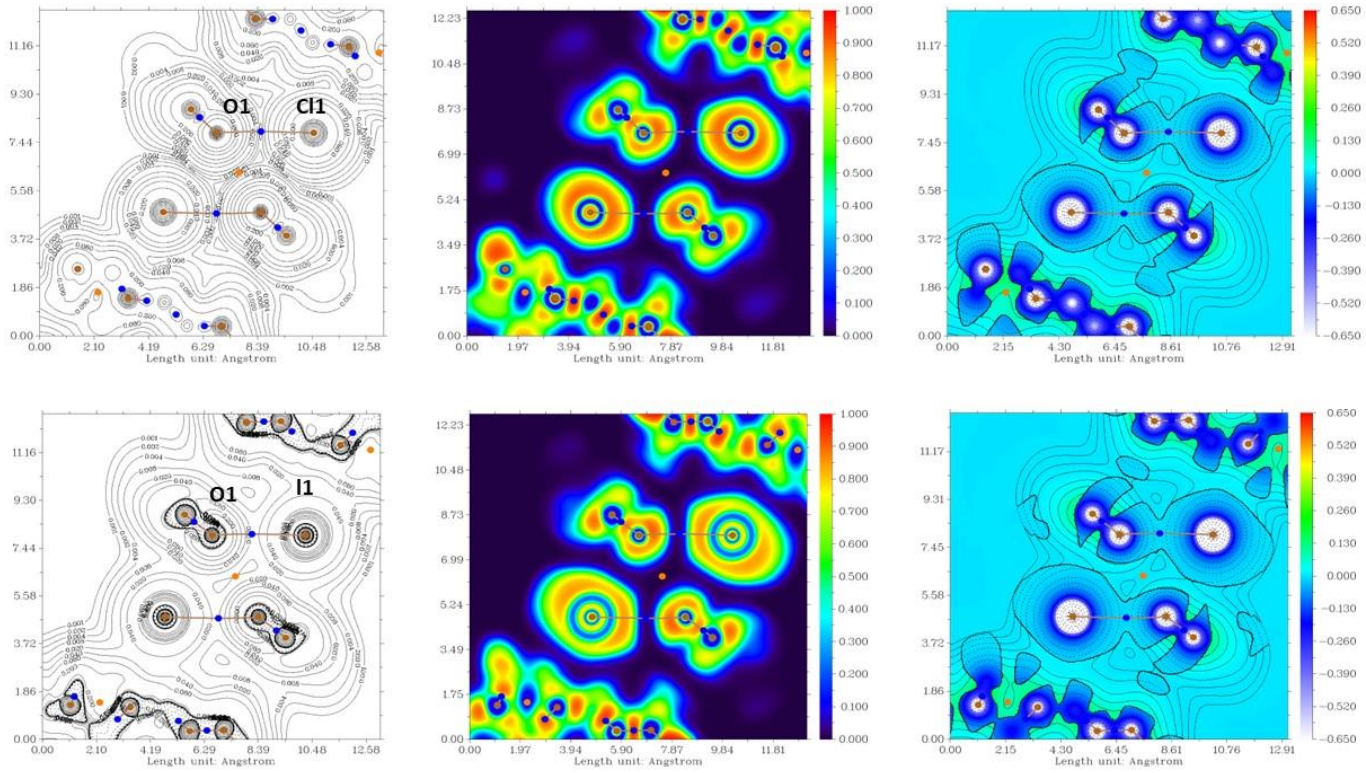

Fig. S15. ∇^2 ρ(**r**) contour (*left column*), ELF (*middle column*) and signλ (*right column*) plots calculated for **2** (above) and **4** (below). Blue dots represent (3,-1) critical points, orange dots represent (3,+1) ring critical points and brown dots represents (3,-3) atomic critical points. Brown lines represent bond paths. Atom labelling is provided only in the ∇^2 ρ(**r**) plots however, view direction in all the depicted plots is identical. Selected energetic and topological parameters: **2**, C21···O1, BCP(3,-1), H_r = 0.124×10^{-2} a.u., E_{int} = 1.10 kcal/mol, signλ = -0.986.10^{-2}; Cl1···O1, BCP(3,-1), H_r = 0.589×10^{-3} a.u., E_{int} = 0.40kcal/mol, signλ = 0.290×10^{-2}, **4**, C21···O1, BCP(3,-1), H_r = 0.926×10^{-3} a.u., E_{int} = 0.50 kcal/mol, signλ = --0.559×10^{-2};I1···O1, BCP(3,-1), H_r = 0.100×10^{-2} a.u., E_{int} = 0.86 kcal/mol, signλ = --0.572×10^{-2}.

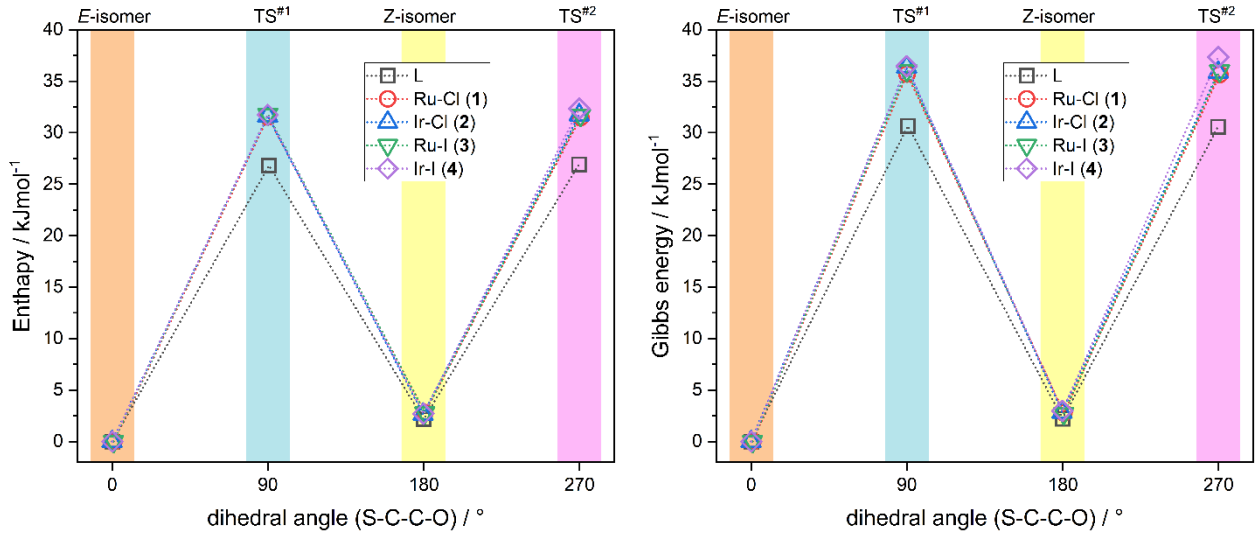

Fig. S16. The graphical comparison of relative enthalpies (*left*) and Gibbs energies (*right*) for ground states of *E*/*Z*-isomers of L1 and **1-4**, and the transition states derived from DFT calculations.

Table S1. Crystallographic data for the reported compounds **1**-**4**.

	1	**2**	**3**
Formula	$C_{21}H_{21}ClF_6N_3OPRuS$	$C_{21}H_{22}ClF_6IrN_3OPS$	$C_{21}H_{21}F_6IN_3OPRuS$
M_r	644.96	737.09	736.41
Crystal system	Monoclinic, *Cc*	Monoclinic, $P2_1/c$	Triclinic, $P\bar{1}$
a /Å	8.8814(6)	12.5825(5)	9.1768(2)
b / Å	22.8613(13)	12.3006(3)	10.2321(2)
c / Å	12.7791(9)	15.4471(6)	15.0893(2)
α / °	90	90	73.270(2)
β / °	109.276(5)	90.752(3)	75.493(2)
γ / °	90	90	78.754(2)
V / Å^3	2449.2(3)	2390.58(15)	1302.03(5)
Z	4	4	2
T / K	100.0(2)	100.0(2)	293(2)
D_c / g cm^{-3}	1.749	2.048	1.878
μ / mm^{-1}	8.215 (CuKa)	13.922 (CuKa)	16.092(CuKa)
F(000)	1288	1424	716
Data/restraints/parameters	4115/2/320	4541/0/321	4723/0/320
Goodness-of-fit (GOF) on F^2	0.895	1.106	1.077
R_1, wR_2 ($I > 2\sigma(I)$) [a, b]	0.0414/0.828	0.0285/0.0687	0.0388/0.1101
R_1, wR_2 (all data) [a, b]	0.0506/0.0842	0.0332/0.0704	0.0399/0.1117
CCDC number	2266585	2266586	2266587

[a] $R_1 = \sum(||F_o| - |F_c||)/\sum|F_o|$, [b] $wR_2 = \{\sum[w(F_o^2 - F_c^2)^2]/\sum[w(F_o^2)^2]\}^{1/2}$

	4
Formula	$C_{21}H_{22}F_6IIrN_3OPS$
M_r	828.54
Crystal system	Monoclinic, $P2_1/c$
a /Å	12.5694(2)
b / Å	12.32870(10)
c / Å	15.6996(2)
α / °	90
β / °	90.5490(10)
γ / °	90
V / Å^3	2432.77(5)
Z	4
T / K	100.0(2)
D_c / g cm^{-3}	2.262
μ / mm^{-1}	22.635 (CuKa)
F(000)	1568
Data/restraints/parameters	80133/0/321
Goodness-of-fit (GOF) on F^2	1.076
R_1, wR_2 ($I > 2\sigma(I)$) [a, b]	0.0504/0.1526
R_1, wR_2 (all data) [a, b]	0.0575/0.1569
CCDC number	2266588

Table S2. The comparisons of DFT calculated selected bond distances[a] and Mayer bond orders for *E*/*Z* isomers of **1**-**4**.[b]

	M-X bond	M-N_{py} bond	M-N_{th} bond
1 $[Ru(\eta^6\text{-pcym})(L1)Cl]^+$	2.410/2.410 [2.394(2)] *0.9374/0.9348*	2.085/2.085 [2.116(10)] *0.6050/0.6064*	2.037/2.037 [2.052(10)] *0.5726/0.5697*
3 $[Ru(\eta^6\text{-pcym})(L1)I]^+$	2.738/2.738 [2.6986(4)] *0.9336/0.9336*	2.082/2.082 [2.120(3)] *0.6140/0.6158*	2.035/2.034 [2.063(3)] *0.5763/0.5736*
2 $[Ir(\eta^5\text{-Cp*})(L1)Cl]$	2.420/2.419 [2.3857(11)] *0.7741/0.7733*	2.112/2.112 [2.114(4)] *0.5050/0.5051*	2.068/2.069 [2.063(4)] *0.5257/0.5223*
4 $[Ir(\eta^5\text{-Cp*})(L1)I]$	2.730/2.731 [2.6445(9)] *0.6679/0.6683*	2.107/2.107 [2.093(8)] *0.5149/0.5150*	2.063/2.063 [2.054(8)] *0.5389/0.5353*

[a] M-X stands for the metal-halogen bond, M-N_{py} stands for the metal-nitrogen bond to the pyridine part of the respective ligand, and M-N_{th} stands for the metal-nitrogen bond to the thiadiazole part of the respective ligand. Bond distances are in Å, and the values in square brackets correspond to the data from X-ray analysis.

[b] Calculated Mayer bond orders are in italics for the respective *E*/*Z* isomers.

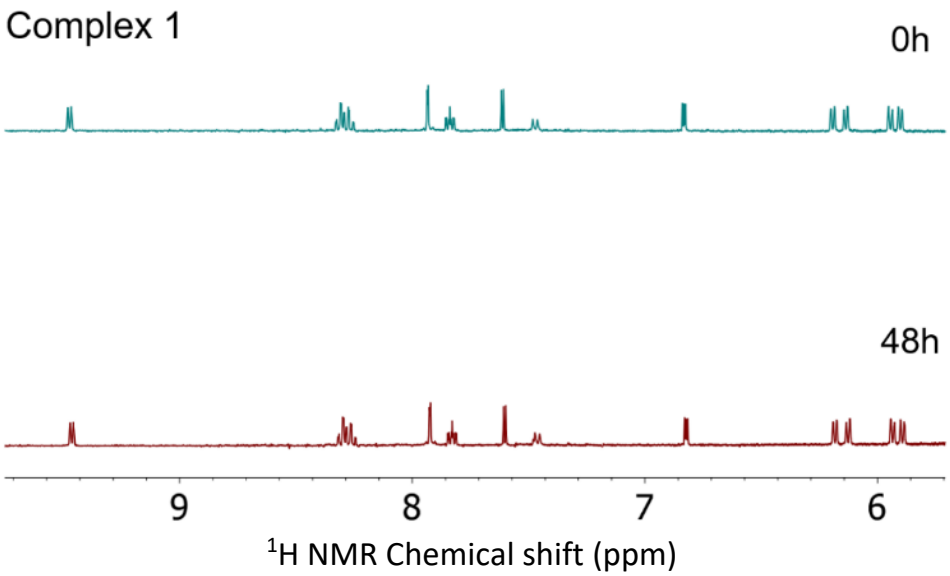

Fig. S17. ^{1}H NMR spectra of complex **1** in SM1 (30% MeOD-d_4/70% D_2O), as observed at different time points (t = 0 or 48h).

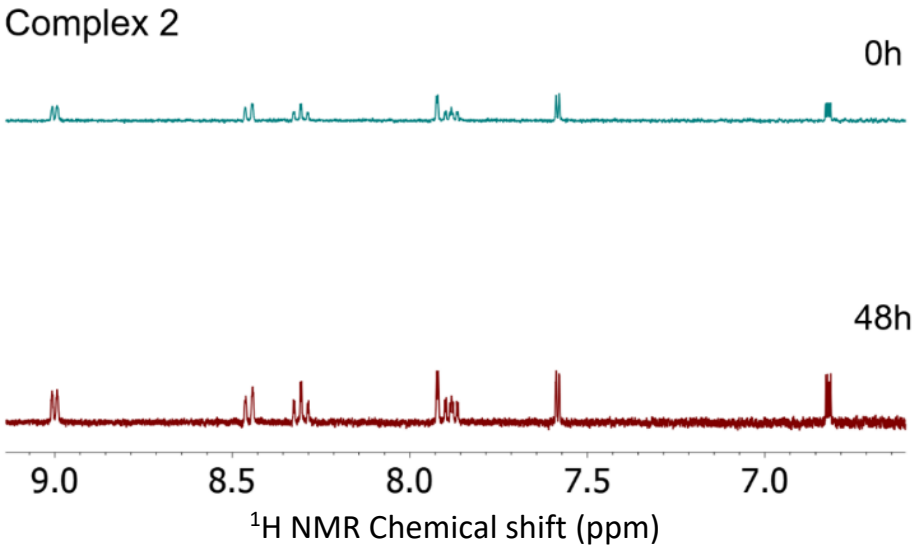

Fig. S18. ^{1}H NMR spectra of complex **2** in in SM1 (30% MeOD-d_4/70% D_2O), as observed at different time points (t = 0 or 48h).

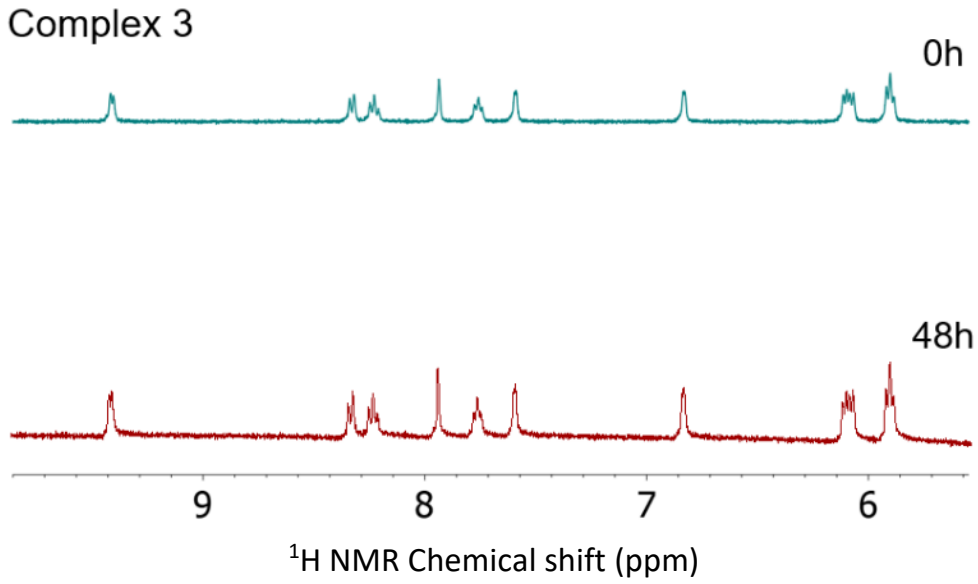

Fig. S19. ^{1}H NMR spectra of complex **3** in in SM1 (30% MeOD-d_4/70% D_2O), as observed at different time points (t = 0 or 48h).

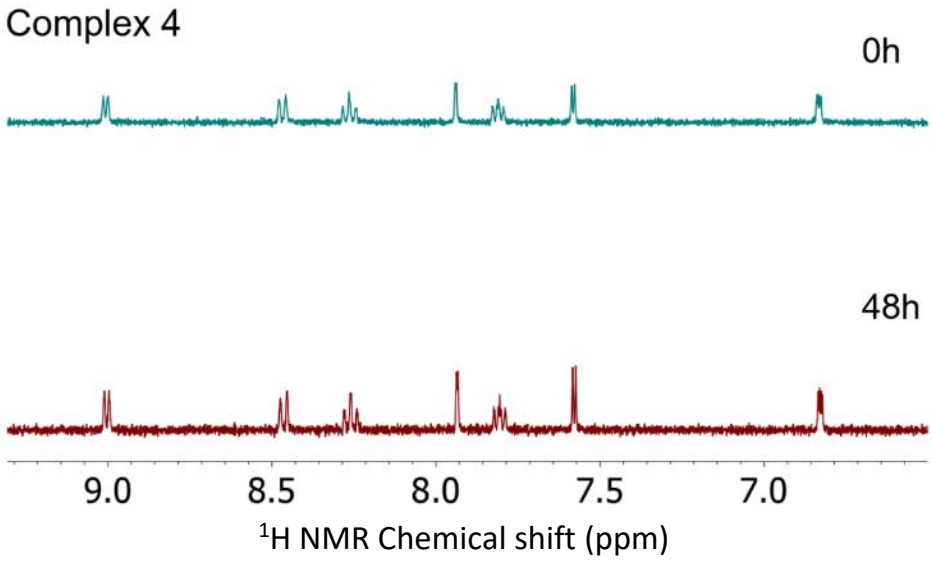

Fig. S20. ^{1}H NMR spectra of complex **4** in in SM1 (30% MeOD-d_4/70% D_2O), as observed at different time points (t = 0 or 48h).

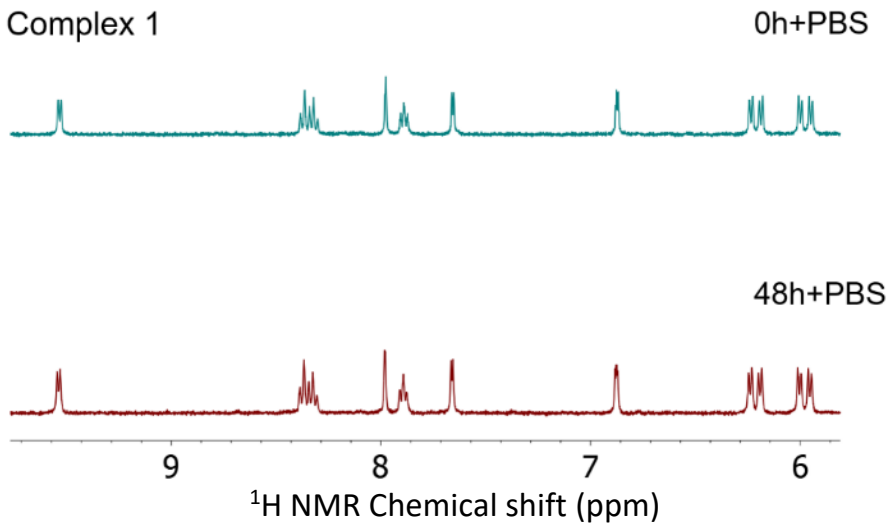

Fig. S21. ^{1}H NMR spectra of complex **1** in SM2 (30% MeOD-d_4/70% of PBS in D_2O (pH=7.4)), as observed at different time points (t = 0 or 48h).

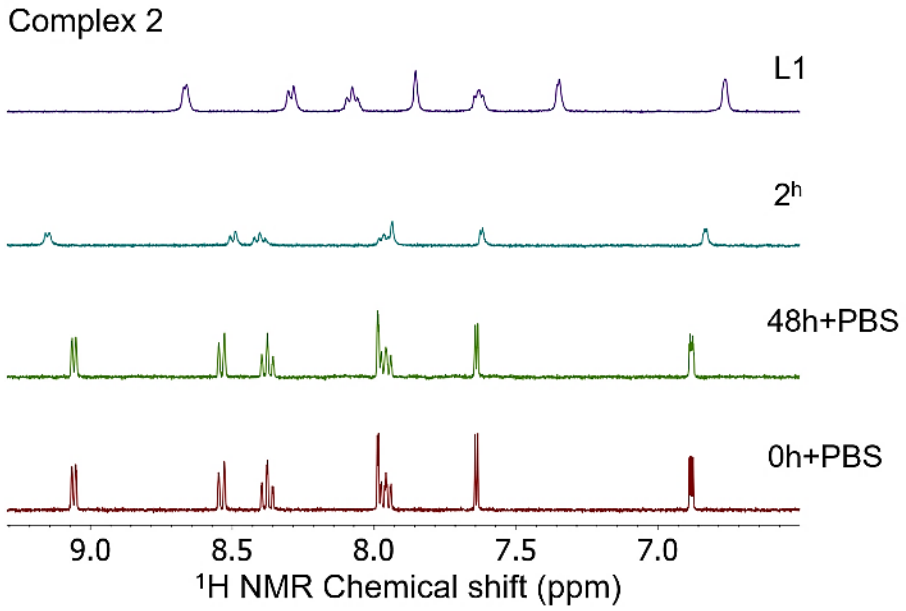

Fig. S22. ^{1}H NMR spectra of complex **2** in SM2 (30% MeOD-d_4/70% of PBS in D_2O (pH=7.4)), as observed at different time points (t = 0 or 48h). Spectra of the dechlorinated species **2^{h}** (in 30% MeOD-d_4/70% D_2O) and ligand L1 (in SM2) are depicted as well for comparative purposes.

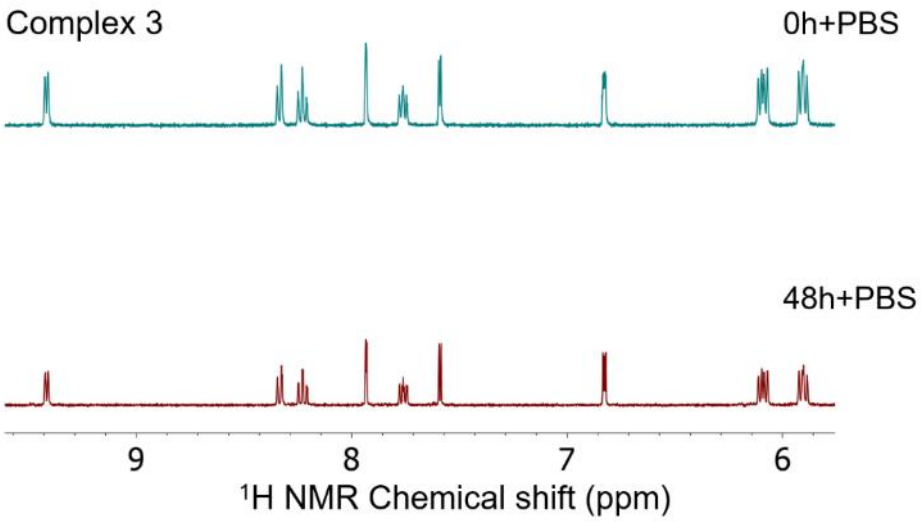

Fig. S23. ^{1}H NMR spectra of complex **3** in SM2 (30% MeOD-d_4/70% of PBS in D_2O (pH=7.4)), as observed at different time points (t = 0 or 48h).

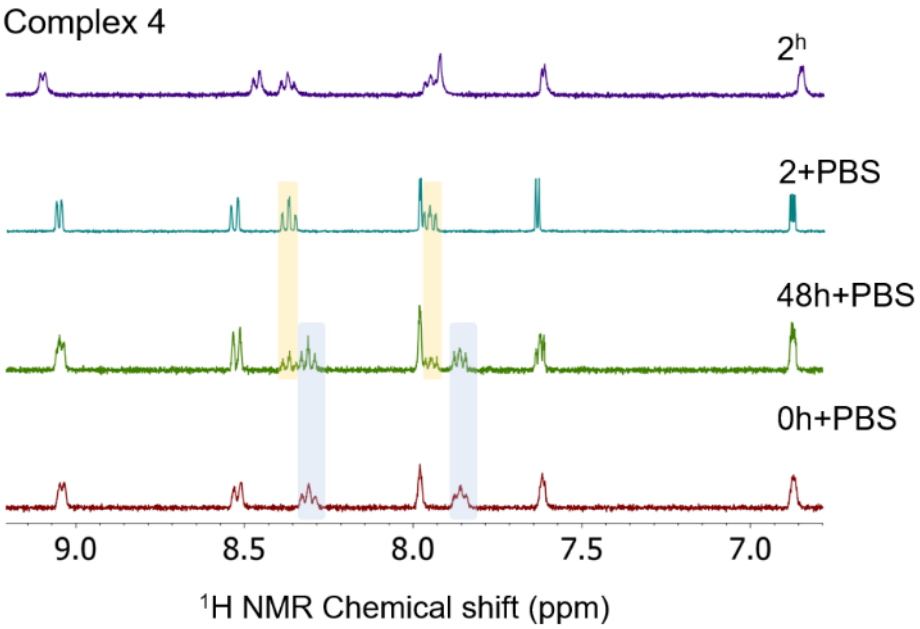

Fig. S24. ^{1}H NMR spectra of complex **4** in SM2 (30% MeOD-d_4/70% of PBS in D_2O (pH=7.4)), as observed at different time points (t = 0 or 48h). Spectra of the dechlorinated species **2^{h}** (in 30% MeOD-d_4/70% D_2O) and complex **2** (in SM2) were depicted as well for comparative purposes, with light blue colour denoting the signals of the original iodido complex and with yellow for the chlorido analogue. Other signals are not coloured due to overlap.

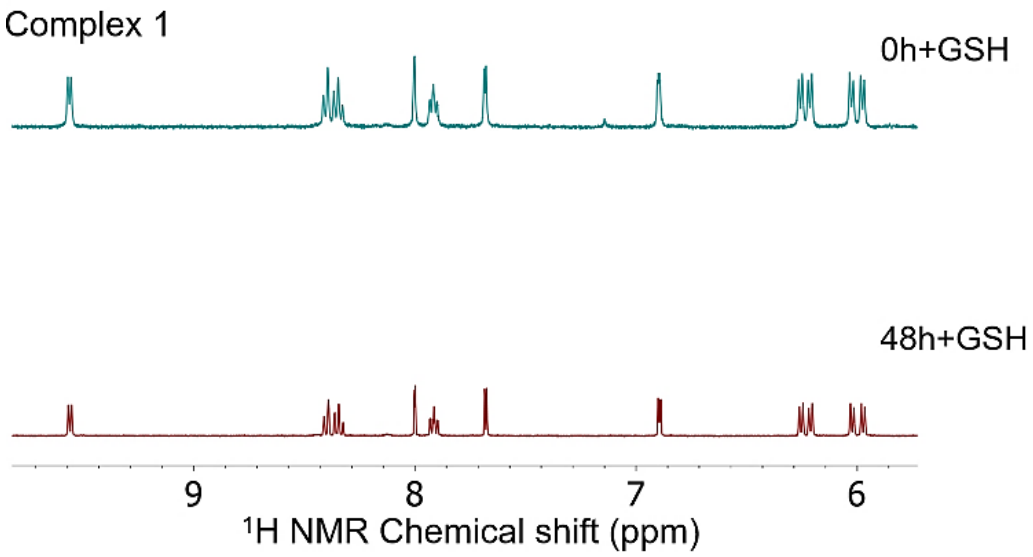

Fig. S25. ^{1}H NMR spectra in the range of 5.7-10 ppm of complex **1** in SM3 (30% MeOD-d_4/70% of PBS in D_2O (pH=7.4) + 5M equivalents of GSH), as observed at different time points (t = 0 or 48h).

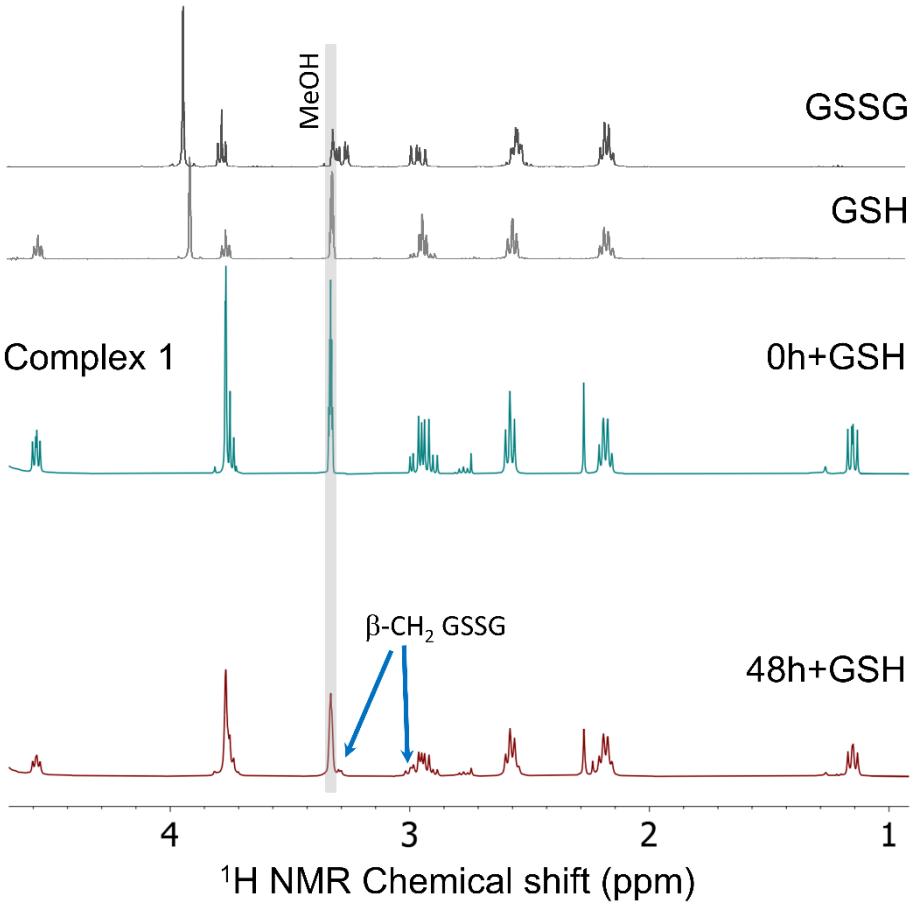

Fig. S26. ^{1}H NMR spectra in the range of 0.9-4.6 ppm of complex **1** in SM3 (30% MeOD-d_4/70% of PBS in D_2O (pH=7.4) + 5M equivalents of GSH), as observed at different time points (t = 0 or 48h). Blue arrows indicate β-CH_2 resonances of oxidized GSH (GSSG). For comparative purposes, the ^{1}H spectra of GSH and GSSG are shown (*top*).

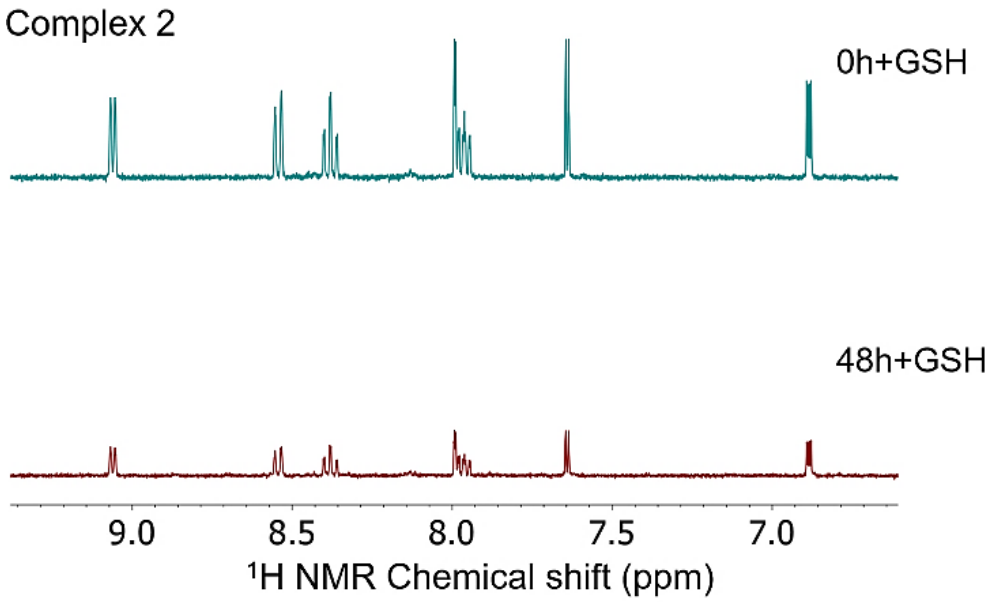

Fig. S27. ^{1}H NMR spectra in the range of 6.5-9.5 ppm of complex **2** in SM3 (30% MeOD-d_4/70% of PBS in D_2O (pH=7.4) + 5M equivalents of GSH), as observed at different time points (t = 0 or 48h).

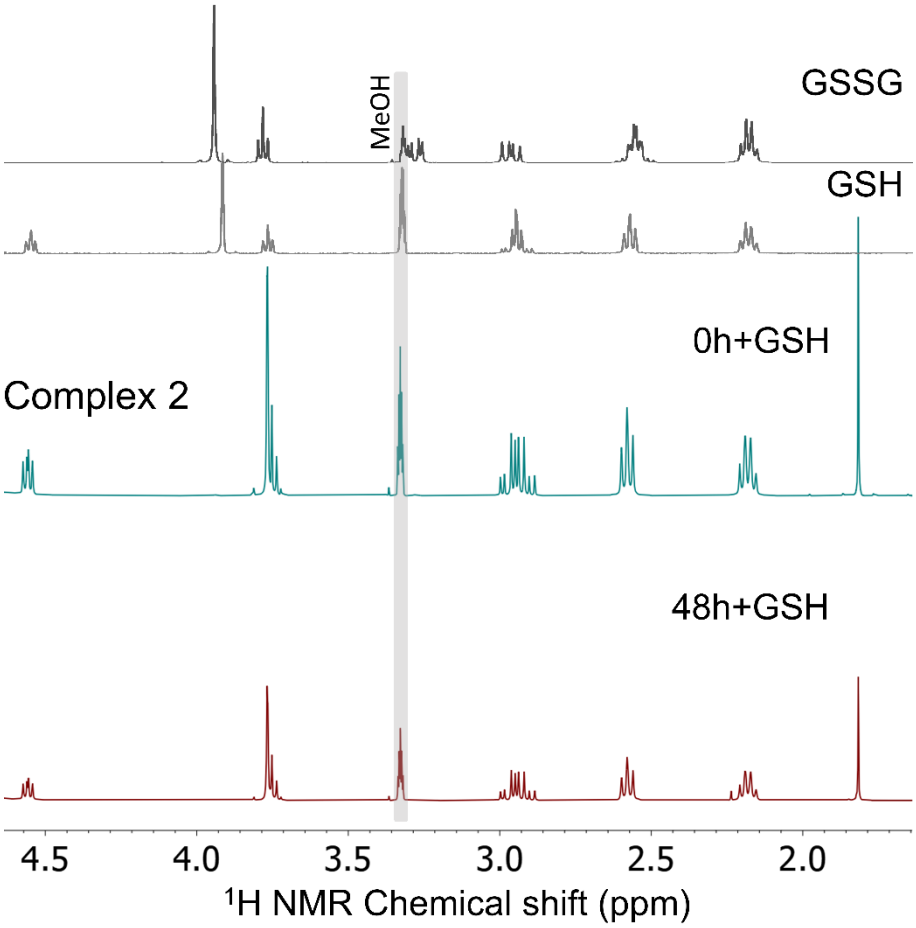

Fig. S28. ^{1}H NMR spectra in the range of 1.1-4.6 ppm of complex **2** in SM3 (30% MeOD-d_4/70% of PBS in D_2O (pH=7.4) + 5M equivalents of GSH), as observed at different time points (t = 0 or 48h). For comparative purposes, the ^{1}H spectra of GSH and GSSG are shown (*top*).

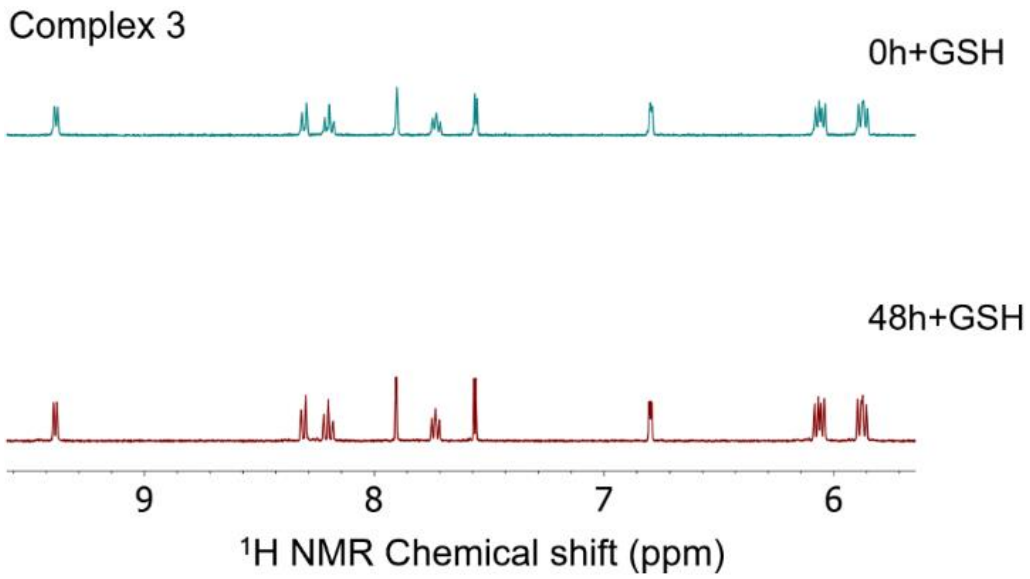

Fig. S29. ^{1}H NMR spectra in the range of 5.7-10 ppm of complex **3** in SM3 (30% MeOD-d_4/70% of PBS in D_2O (pH=7.4) + 5M equivalents of GSH), as observed at different time points (t = 0 or 48h).

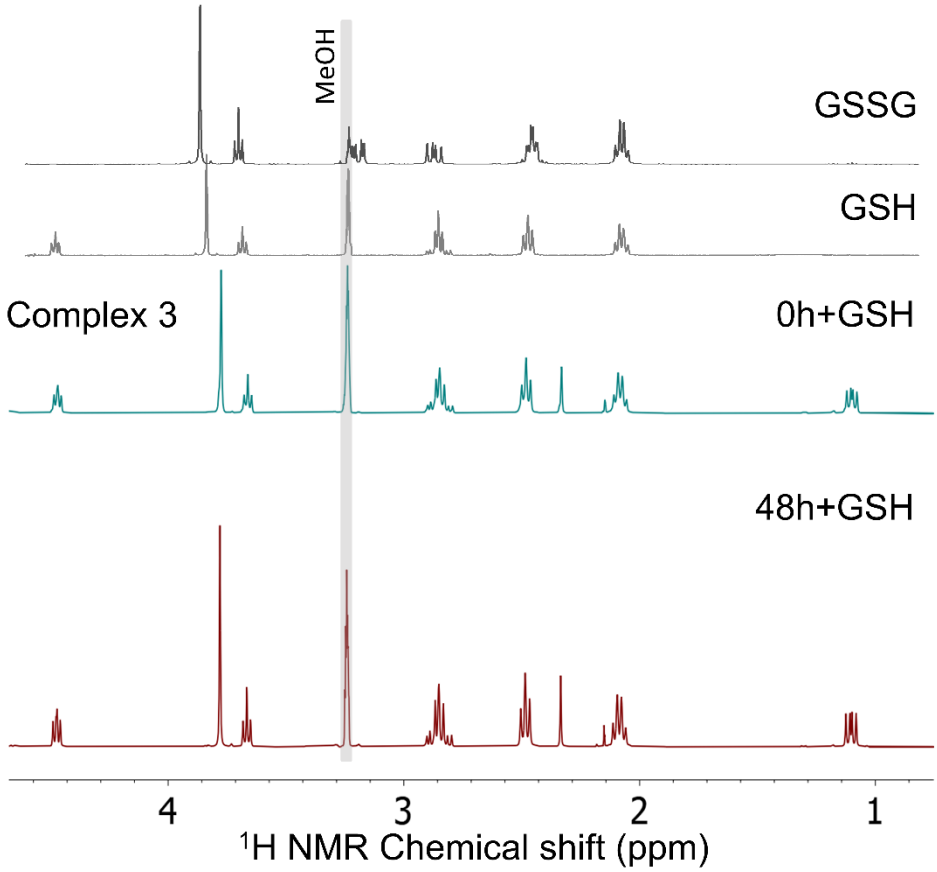

Fig. S30. ^{1}H NMR studies in the range of 0.9-4.6 ppm of complex **3** in SM3 (30% MeOD-d_4/70% of PBS in D_2O (pH=7.4) + 5M equivalents of GSH), as observed at different time points (t = 0 or 48h). For comparative purposes, the ^{1}H spectra of GSH and GSSG are shown (*top*).

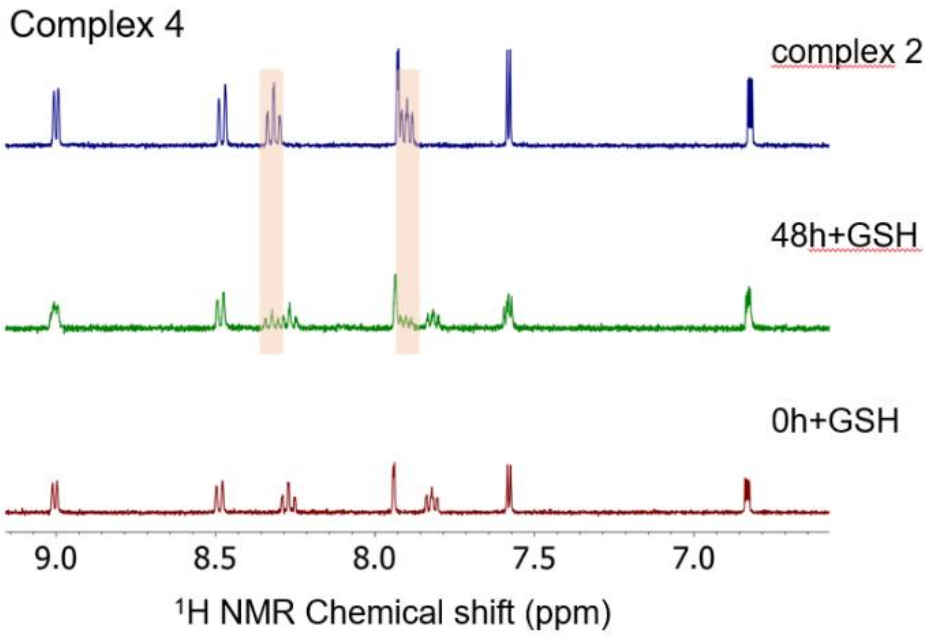

Fig. S31. ^{1}H NMR spectra in the range of 6.5-9.2 ppm of complex **4** in SM3 (30% MeOD-d_4/70% of PBS in D_2O (pH=7.4) + 5M equivalents of GSH), as observed at different time points (t = 0 or 48h). A spectrum of **2** in the same medium is depicted for comparative purposes. Orange areas denote discreet signals belonging to chlorido complex, other signals are not highlighted due to overlap.

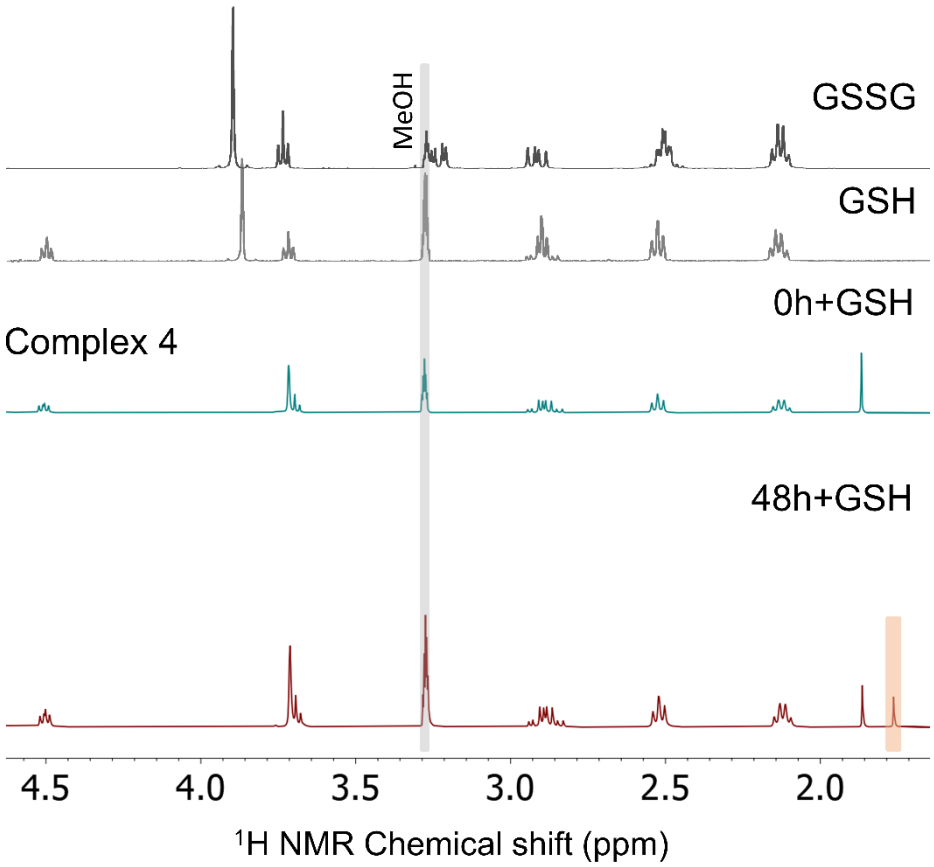

Fig. S32. ^{1}H NMR studies in the range of 1.6-4.6 ppm of complex **4** in SM3 (30% MeOD-d_4/70% of PBS in D_2O (pH=7.4) + 5M equivalents of GSH), as observed at different time points (t = 0 or 48h). Orange area denotes a Cp* signal belonging to chlorido complex. For comparative purposes, the ^{1}H spectra of GSH and GSSG are shown (*top*).

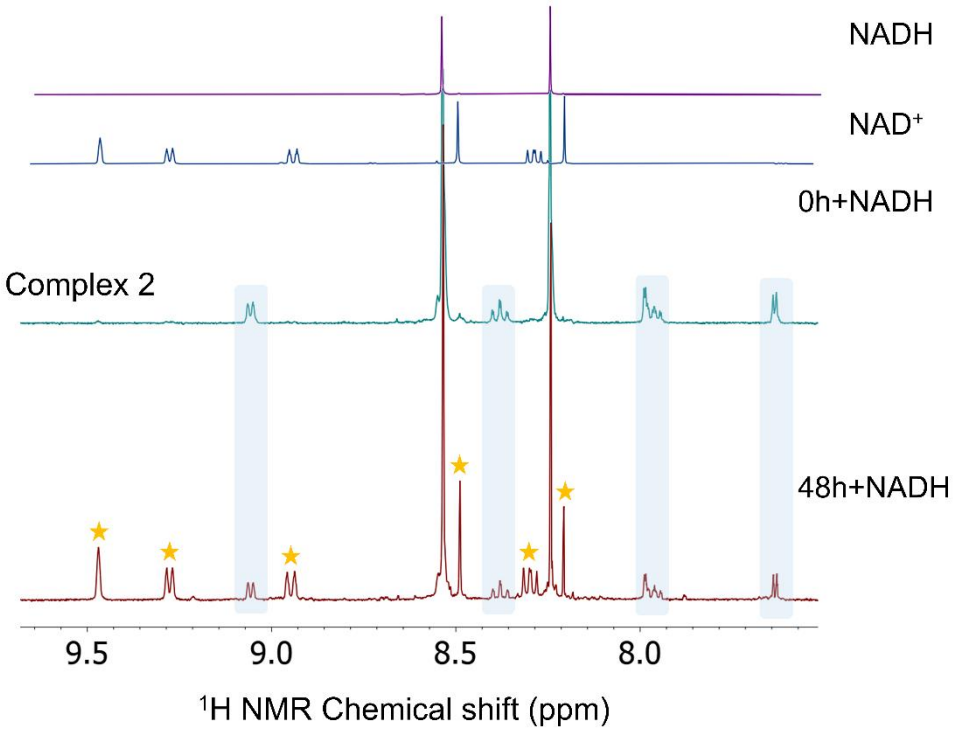

Fig. S33. ^{1}H NMR studies of complex **2** in SM4 (30% MeOD-d_4/70% of PBS in D_2O (pH=7.4) + 5M equivalents of NADH), as observed at different time points (t = 0 or 48h). Asterisks denote the signals of NAD^+ originating from oxidation of NADH in the mixture with **2**. Blue areas mark the signals of **2**. For comparative purposes, the ^{1}H spectra of NADH and NAD^+ are shown (*top*).

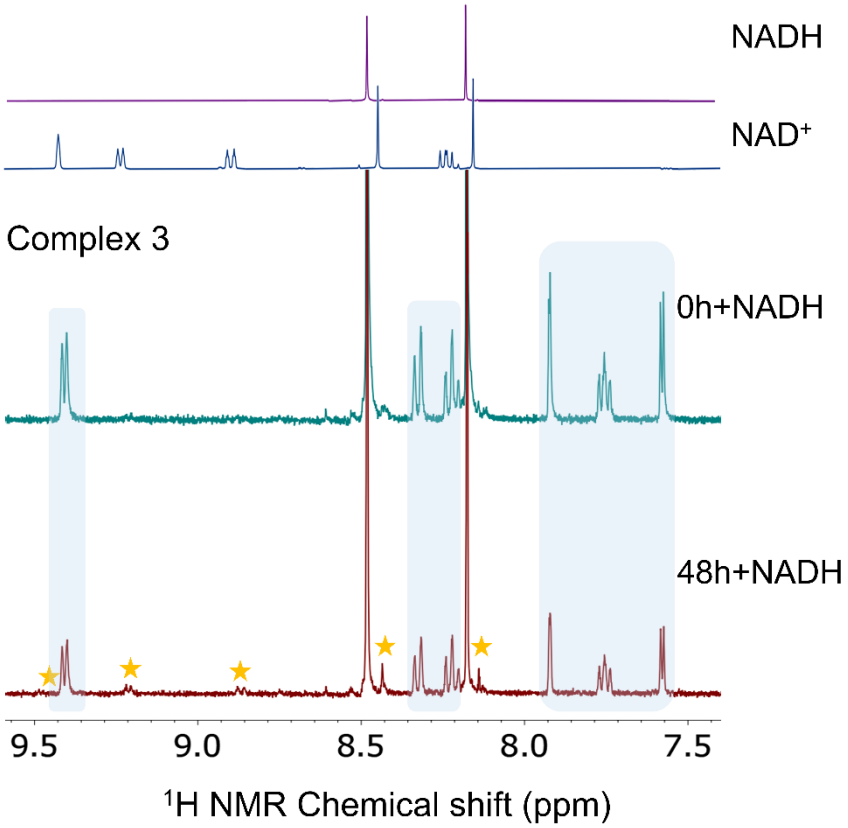

Fig. S34. ^{1}H NMR studies of complex **3** in SM4 (30% MeOD-d_4/70% of PBS in D_2O (pH=7.4) + 5M equivalents of NADH), as observed at different time points (t = 0 or 48h). Asterisks denote the signals of NAD^+ originating from oxidation of NADH in the mixture with **3**. Blue areas mark the signals of **3**. For comparative purposes, the ^{1}H spectra of NADH and NAD^+ are shown (*top*).

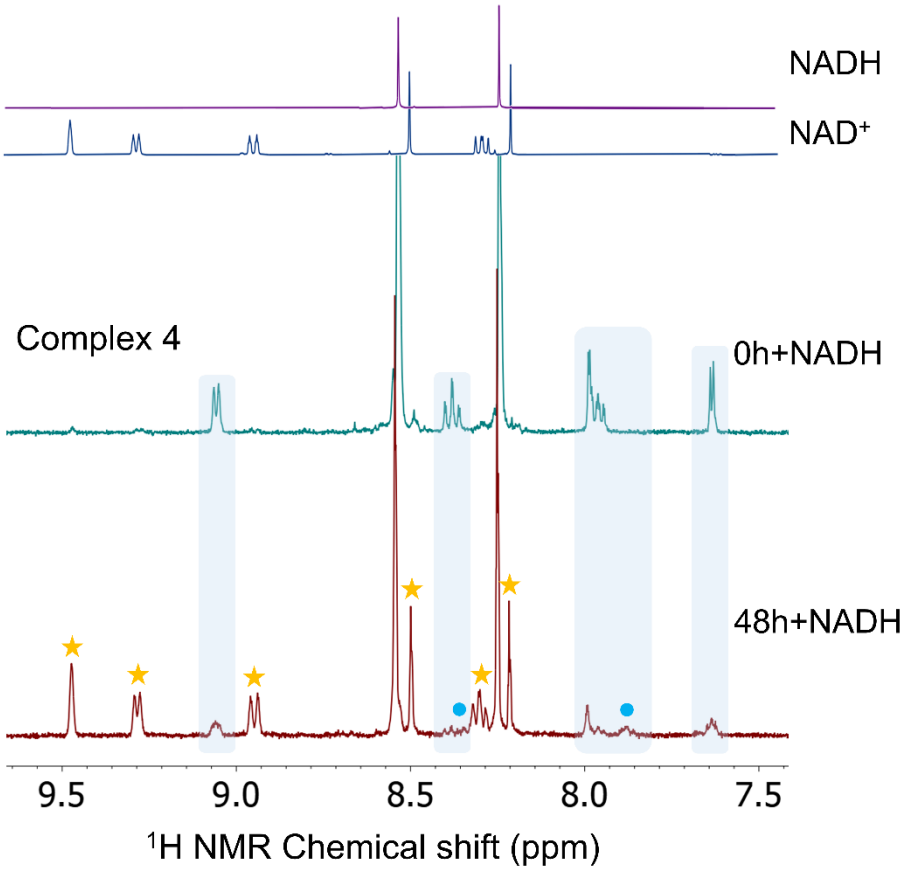

Fig. S35. ^{1}H NMR studies of complex **4** in SM4 (30% MeOD-d_4/70% of PBS in D_2O (pH=7.4) + 5M equivalents of NADH), as observed at different time points (t = 0 or 48h). Asterisks denote the signals of NAD^+ originating from oxidation of NADH in the mixture with **4**. Blue areas mark the signals of **4**, with blue circles indicating discreet signals of chlorido complex. For comparative purposes, the ^{1}H spectra of NADH and NAD^+ are shown (*top*).

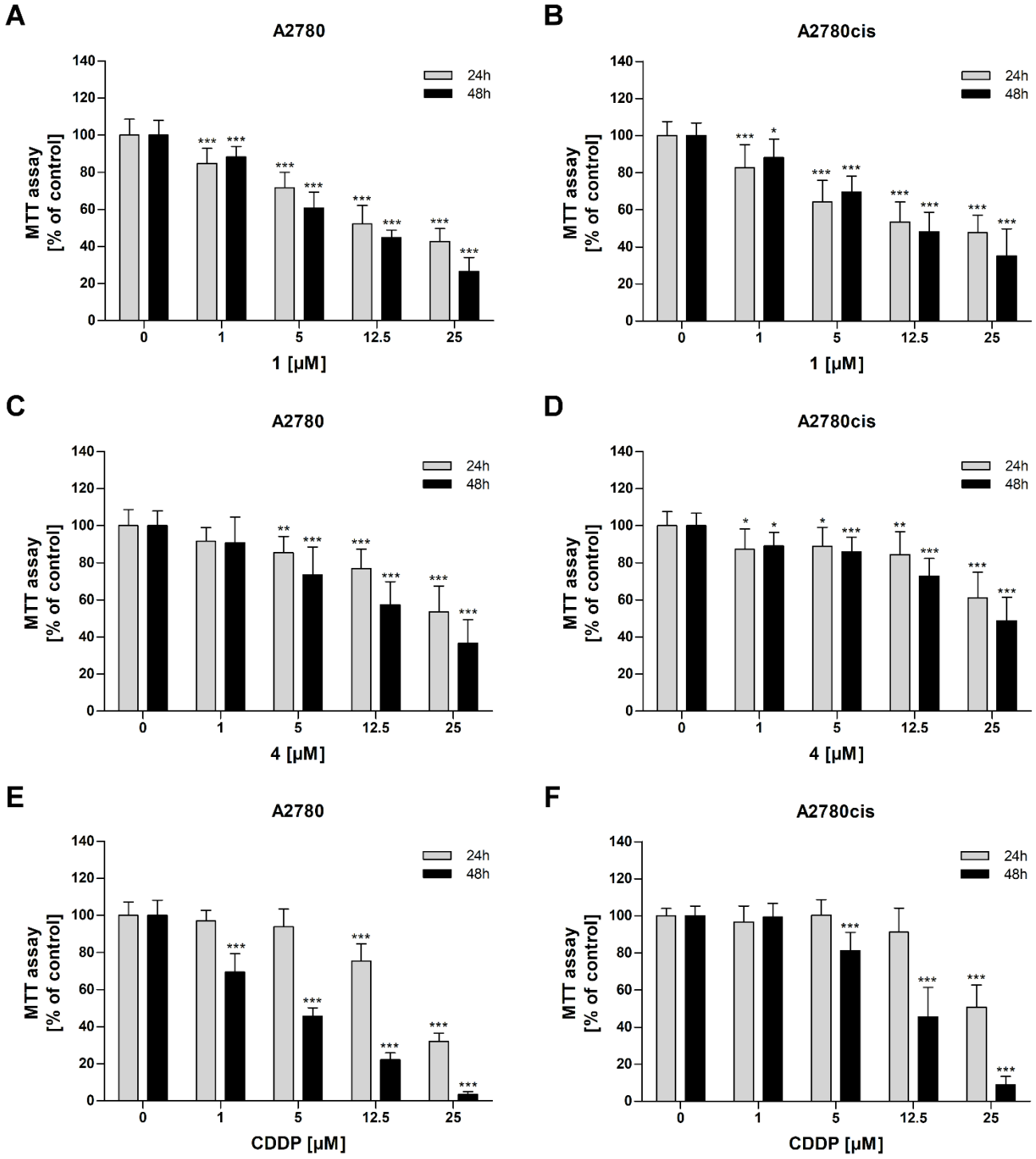

Fig. S36 The effect of **1** (*top A, B*), **4** (*middle C, D*) and CDDP (*bottom E, F*) on metabolic activity (MTT assay) of A2780 and A2780cis ovarian carcinoma cell lines. Metabolic activity was analysed 24 and 48h after treatment of cells with selected complexes. The experimental groups were compared with untreated control (* $p < 0.05$, ** $p < 0.01$, *** $p < 0.001$).

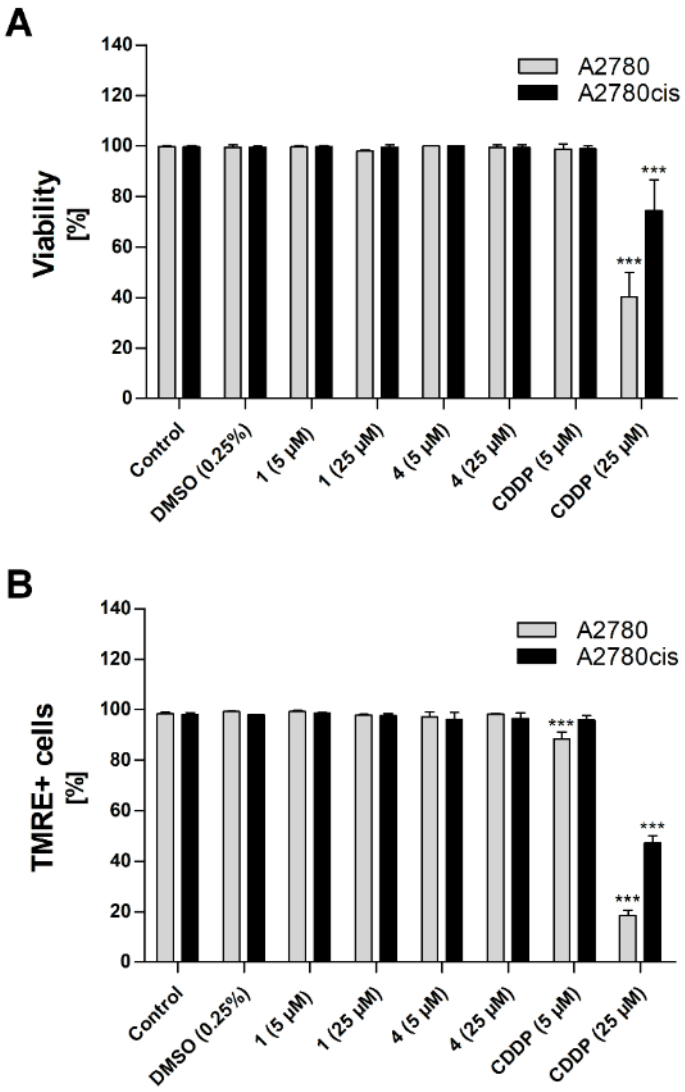

Fig. S37. Effect of **1**, **4** and CDDP on changes in viability (A) and mitochondrial membrane potential (B) of A2780 and A2780cis ovarian carcinoma cell lines. TMRE+ cells represent cells with normal mitochondrial membrane potential. Viability and mitochondrial membrane potential were analysed 48h after treatment of cells with selected complexes. The experimental groups were compared with untreated control (*** $p < 0.001$).

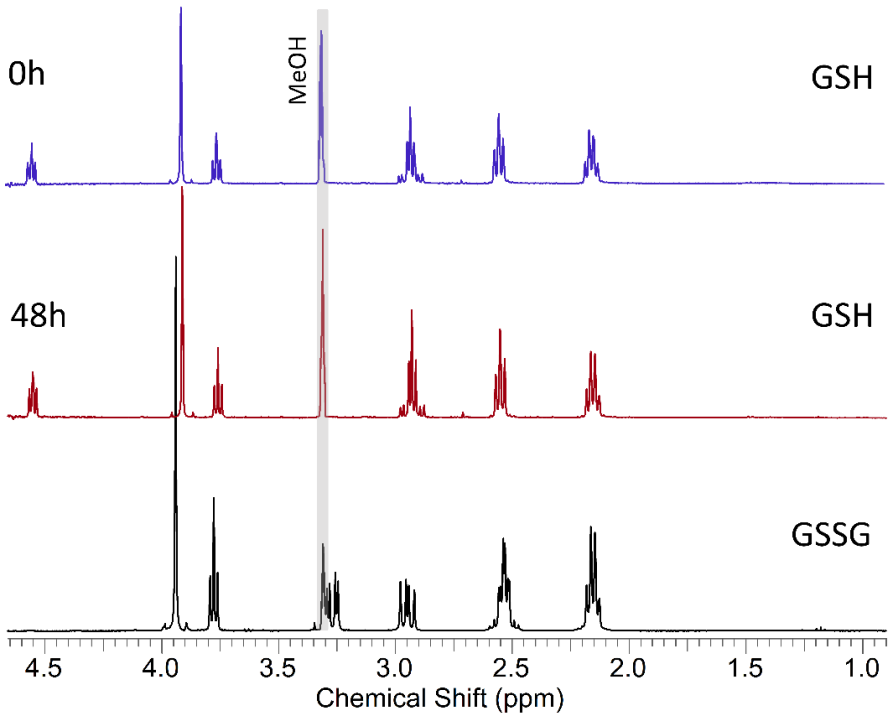

Fig. S38. Control experiments showing the ^{1}H NMR spectra of GSH in 30% MeOD-d_4/70% of PBS in D_2O (pH=7.4) at different time points (t = 0 or 48h) measured under the same experimental conditions as for the interaction experiments with **1**-**4**. No changes are observed. For comparative purposes, the ^{1}H spectrum of GSSG is shown (*bottom*).

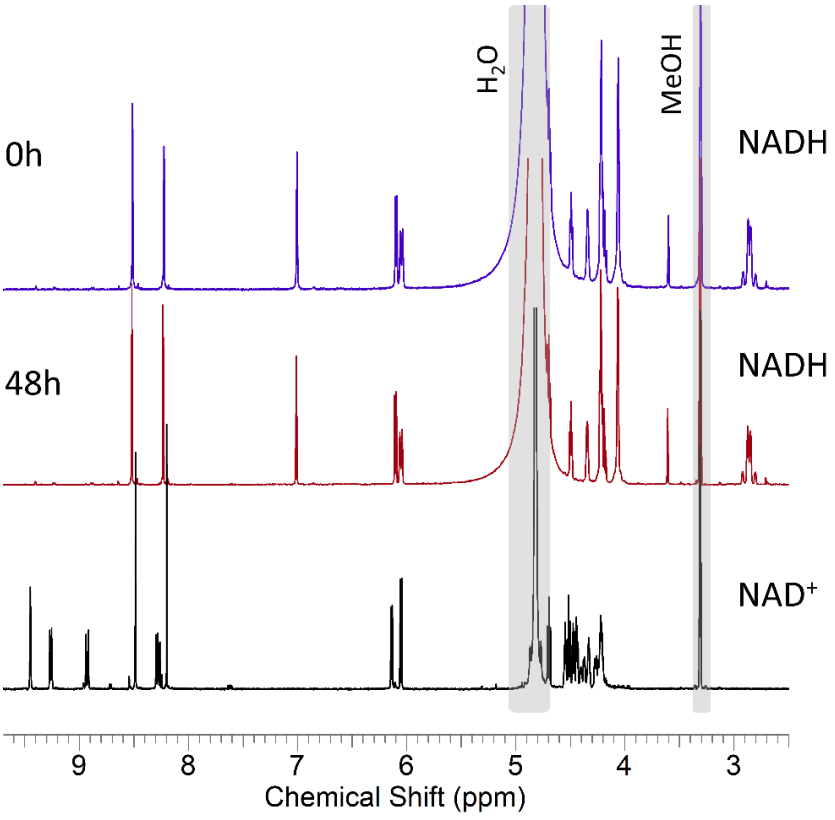

Fig. S39. Control experiments showing the ^{1}H NMR spectra of NADH in 30% MeOD-d_4/70% of PBS in D_2O (pH=7.4) at different time points (t = 0 or 48h) measured under the same experimental conditions as for the interaction experiments with **1**-**4**. No changes are observed. For comparative purposes, the ^{1}H spectrum of NAD^+ is shown (*bottom*).